# Chapter 6
## Low Cycle Fatigue Behavior at 300 °C

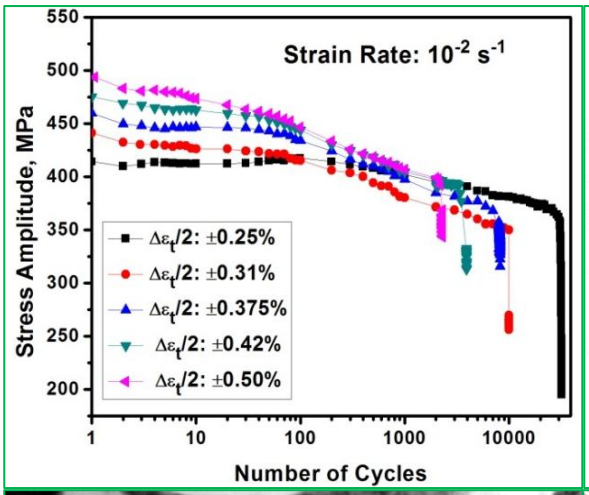


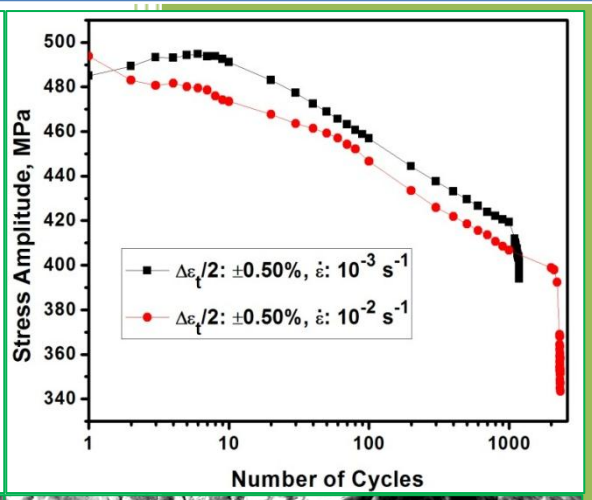


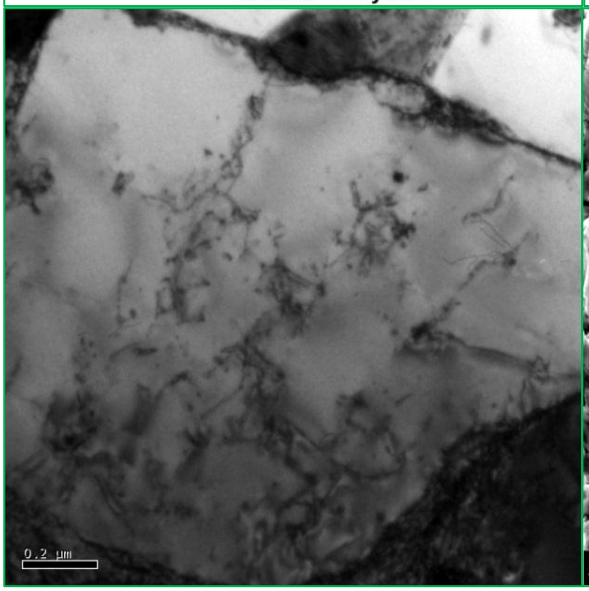


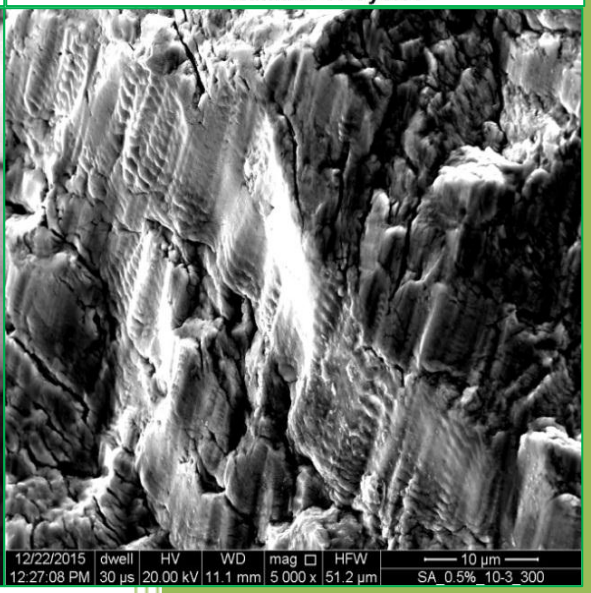

## 6.1 Introduction

In this chapter LCF behavior is presented at 300 °C in the temperature range of dynamic strain ageing (DSA) over a wide range of strain amplitudes from ±0.25% to ±0.50%, at two different strain rates of $10^{-2}$ $s^{-1}$ & $10^{-3}$ $s^{-1}$. Inverse effect of strain rate is observed on LCF behavior such as increase in cyclic stress response, reduction in fatigue life and decrease in plastic strain amplitude with decrease in strain rate. Irrespective of the strain rate and strain amplitude there is cyclic softening till failure of the specimen. Bowing of dislocations is seen at low strain rate of $10^{-3}$ $s^{-1}$. The observed cyclic softening irrespective of strain amplitude and strain rate, is attributed mainly to formation of cell structure and dynamic recovery. The increase in fatigue crack growth at strain rate of $10^{-3}$ $s^{-1}$ is due to DSA.

## 6.2 Cyclic Stress Response

Variation of cyclic stress amplitude with number of cycles for different strain amplitudes, at strain rates of $10^{-2}$ and $10^{-3}$ $s^{-1}$, is shown in Figs. 6.1 a & b respectively. It is seen from figure 6.1a that there is stabilization of stress during the initial few cycles followed by lowering of stress amplitude reflecting cyclic softening till failure, at low strain amplitudes at strain rate of $10^{-2}$ $s^{-1}$. With increase in strain amplitude there is mild hardening during the initial few cycles, followed by softening. The number of cycles during the initial stabilization/mild hardening decreased with increase in strain amplitude. The rate of cyclic softening increases with increase in strain amplitude. A similar type of behavior is observed also at the lower strain rate of $10^{-3}$ $s^{-1}$.

Effect of strain rate on cyclic stress response for the strain amplitude of ±0.50% is shown in Fig. 6.2. In general, cyclic stress amplitude decreased with decrease in strain

rate. However, an inverse stress response may be seen from figure 6.2 in which the stress amplitude is increases with decrease in strain rate from $10^{-2}$ $s^{-1}$ to $10^{-3}$ $s^{-1}$.

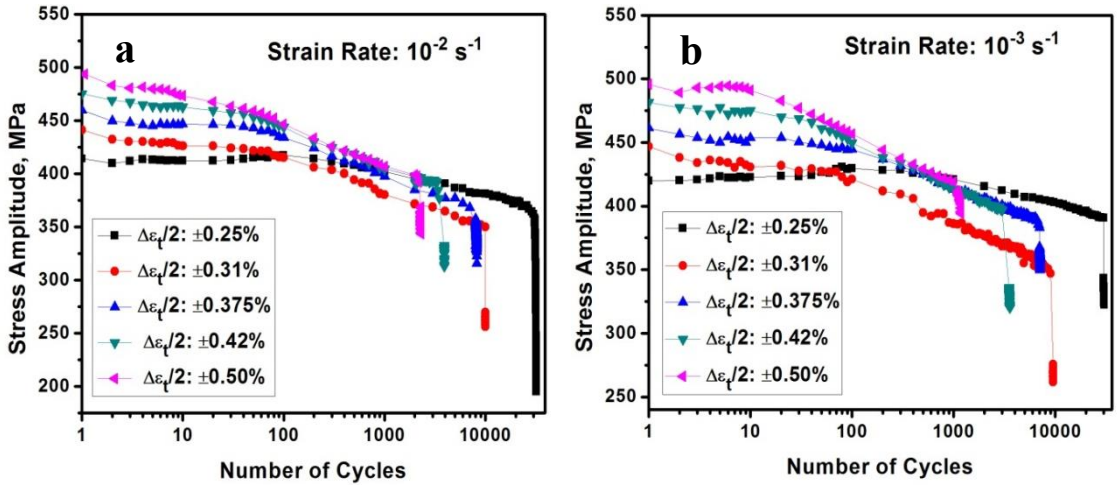


**Fig. 6.1** Variation of cyclic stress with number of cycles for different strain amplitudes at different strain rates: (a) $10^{-2}$ $s^{-1}$, and (b) $10^{-3}$ $s^{-1}$.

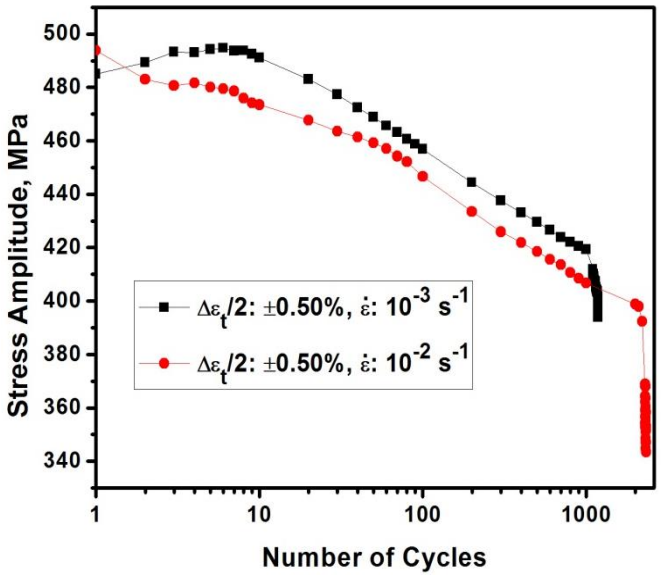


**Fig. 6.2** Effect of strain rate on cyclic stress response at strain amplitude of ±0.50%.

The extent of initial hardening also increased at the lower strain rate. The number of cycles to failure ($N_f$) expressed as number of reversals to failure ($2N_f$)

reduced markedly with decrease in the strain rate (Fig. 6.2). Plastic strain amplitude for the specimen tested at high strain amplitude of ±0.50% for both the strain rates is recorded in Table 6.1. There is decrease in plastic strain amplitude ($\Delta\varepsilon_p/2$) at the lower strain rate of $10^{-3}$ $s^{-1}$.

**Table 6.1** LCF parameters at different strain rates of $10^{-2}$ $s^{-1}$ & $10^{-3}$ $s^{-1}$.

| Sl. No. | Strain Rate ($s^{-1}$) | Frequency (Hz) | $\Delta\varepsilon_t/2$ (%) | $\Delta\varepsilon_p/2$ (%) | $N_f$ (Cycles) |
|---|---|---|---|---|---|
| 1 | $10^{-2}$ | 0.50 | ±0.50 | 0.25 | 2300 |
| 2 | $10^{-3}$ | 0.05 | ±0.50 | 0.20 | 1185 |

## 6.3 Dependence of Fatigue Life on Plastic Strain Amplitude

The variation of reversals to failure ($2N_f$) with plastic strain amplitude ($\Delta\varepsilon_p/2$) is shown on logarithmic scale in Fig. 6.3. It is obvious that there is linear variation of $2N_f$

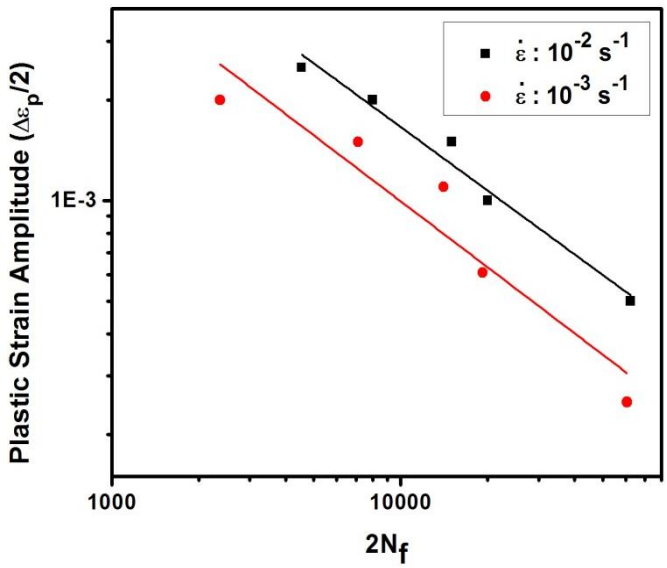


**Fig. 6.3** Coffin–Manson plot at strain rates of $10^{-2}$ $s^{-1}$ and $10^{-3}$ $s^{-1}$ at 300 °C.

with $\Delta\varepsilon_p/2$ at both the strain rates. The LCF parameter are determined using the Coffin–Manson relationship [131] and are presented in Table 6.2. Decrease in fatigue life with decrease in strain rate may also be seen from the Fig. 6.3 and is also reflected from the higher ductility exponent (c) and lower fatigue ductility coefficient ($\varepsilon_f'$).

**Table 6.2** LCF parameters at different strain rates.

| **Strain Rate ($s^{-1}$)** | **Fatigue Ductility Coefficient ($\varepsilon_f'$)** | **Fatigue Ductility Exponent** (c) |
|---|---|---|
| $\mathbf{10^{-2}}$ | 0.56 | -0.63 |
| $\mathbf{10^{-3}}$ | 0.41 | -0.65 |

## 6.4 Masing and Non–Masing Behavior

In order to examine whether a material exhibits Masing or non–Masing behavior, the lower tips of stable hysteresis loops corresponding to different strain amplitudes of the LCF tests, are translated to a common origin. Translated hysteresis loops corresponding to half–life for the different strain amplitudes are shown in Fig.6.4. There is similar type of behavior like that at RT. It is obvious from this figure that this steel exhibits non–Masing behavior at low strain level of ±0.25% and Masing behavior at high strain amplitudes (≥ ±0.375%). Thus, the critical strain amplitude for the transition from non–Masing to Masing behavior is ±0.375%.

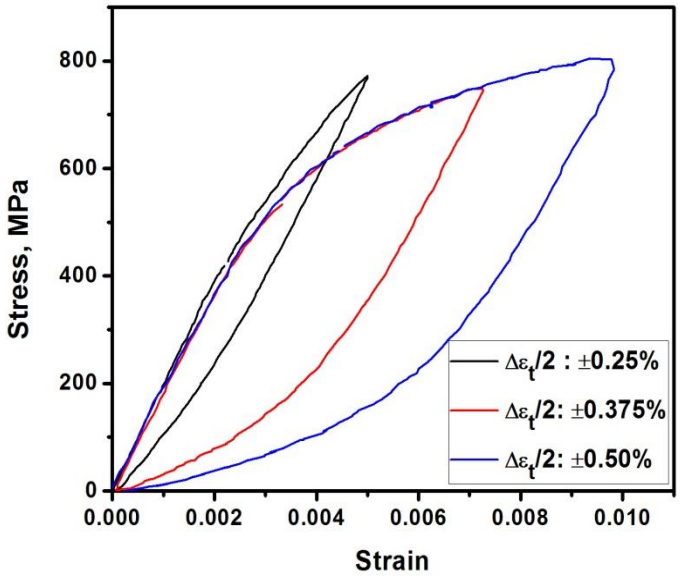


**Fig. 6.4** Translated hysteresis loops to a common point of maximum compressive stress showing non–Masing behavior at the lowest strain amplitude of ±0.25% and Masing behavior at high strain amplitudes (≥ ±0.375%).

## 6.5 Deformation Behavior

Dislocation substructures of the fatigue tested specimens at different strain amplitudes, at strain rate of $10^{-2}$ $s^{-1}$, are shown in Fig. 6.5 a–c. During cyclic deformation the tempered lath structure with high dislocation density (Fig. 3.1c & d) is transformed into low energy cell structure.

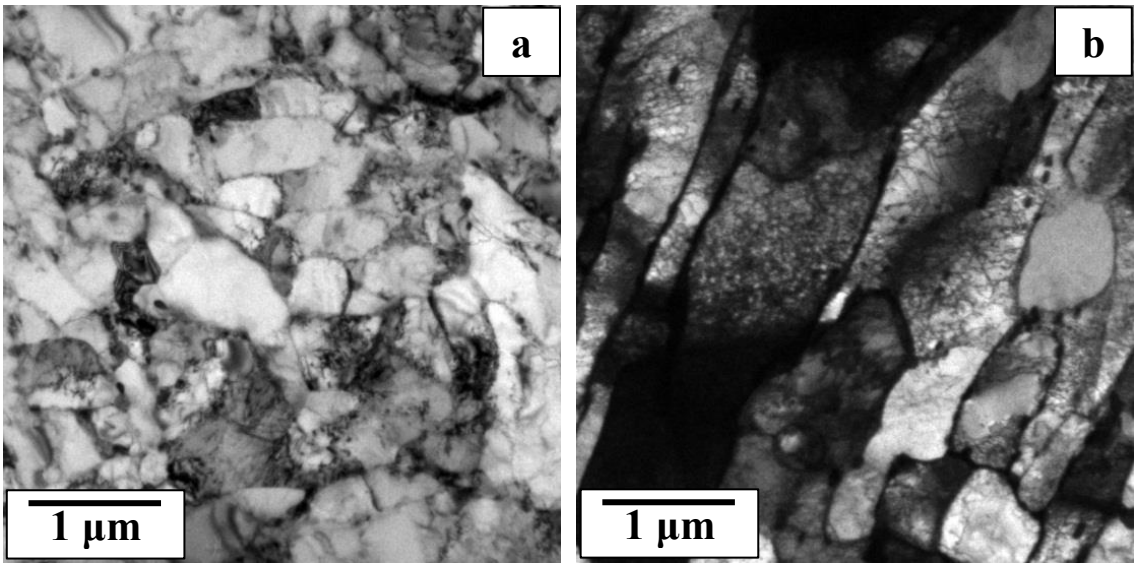

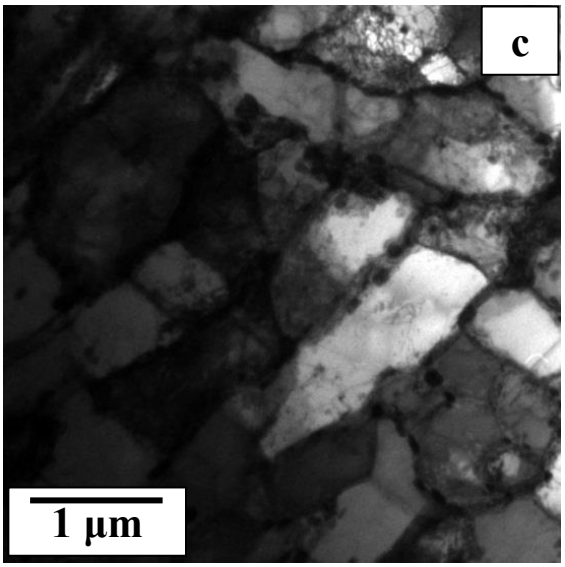


**Fig. 6.5** Dislocation substructure of the specimens tested at strain rate of $10^{-2}$ $s^{-1}$ for different strain amplitudes: (a) tested at ±0.25%, (b) ±0.375%, & (c) ±0.50%.

At low strain amplitude of ±0.25% equiaxed but not well defined cell structure is observed (Fig. 6.5a). There is also low dislocation density at low strain amplitude. On the other hand, at high strain amplitudes of ±0.375% & ±0.50%, elongated cell structure is observed and dislocation density in cell walls is also increased (Fig. 6.5 c & d). Dislocation–precipitate interaction may be seen in Fig.6.5 c.

Bright field TEM micrograph of the fatigue tested specimens at strain rate of $10^{-3}$ $s^{-1}$ is shown in Fig. 6.6. Similar type of deformation behavior is observed also at the low strain rate of $10^{-3}$ $s^{-1}$ with elongated structure at the higher strain amplitudes (Fig. 6.6). Thus, it is evident that there was transition from equiaxed to elongated cell structure with increase in strain amplitude to ±0.375% at both the strain rates.

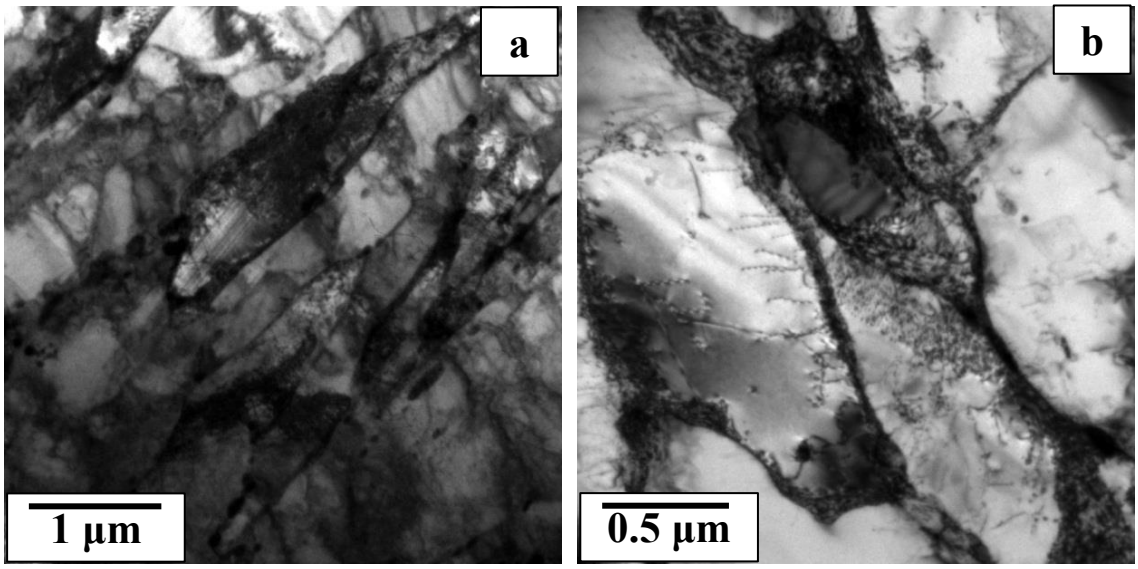


**Fig. 6.6** Bright field TEM micrograph showing dislocation configuration resulting from LCF test at strain rate of $10^{-3}$ $s^{-1}$ at strain amplitudes of (a) ±0.375%, (b) ±0.50%.

## 6.6 Fracture Behavior

Effect of strain amplitude and strain rate on fracture behavior of the LCF tested at 300 °C is shown Figs. 6.7–6.11. There is significant effect of strain rate and strain amplitude on fracture behavior of the steel. Overall view of the fracture surfaces of the specimens tested at strain amplitudes of ±0.25% and ±0.5% at strain rates of $10^{-2}$ $s^{-1}$ and $10^{-3}$ $s^{-1}$ are shown in Fig. 6.7 and 6.8 respectively. Crack initiation point is marked by white arrow and the region of fatigue crack propagation is shown by dotted line. It is obvious from these figures that area due to fatigue crack propagation is decreased at low strain rate of $10^{-3}$ $s^{-1}$. At high strain amplitude of ±0.50% there is single crack initiation at high strain rate of $10^{-2}$ $s^{-1}$ (Fig. 6.7b). On the other hand, there are multiple crack initiation points at the same strain amplitude but at low strain rate of $10^{-3}$ $s^{-1}$ (Fig. 6.8b). Magnified views of the fatigue crack propagation region at strain amplitudes from ±0.25% to ±0.50%, at strain rates of $10^{-2}$ $s^{-1}$ & $10^{-3}$ $s^{-1}$, are shown in Figs. 6.9 and 6.10 respectively.

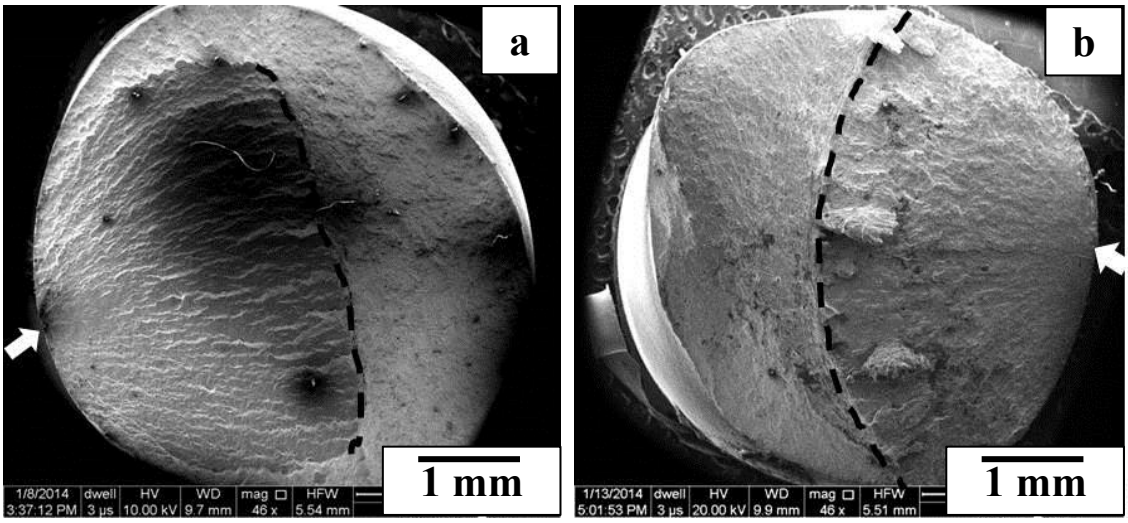


**Fig. 6.7** Fracture surface of the fatigue specimens tested at strain rate of $10^{-2}$ $s^{-1}$ at strain amplitudes of (a) ±0.25%, (b) ±0.50%.

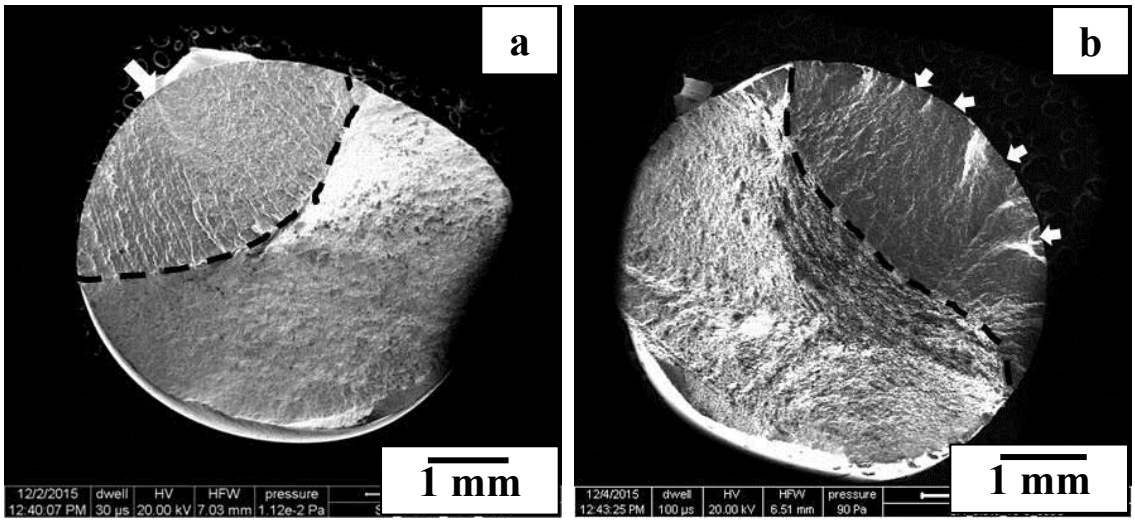


**Fig. 6.8** Fracture surface of the fatigue specimen tested at strain rate of $10^{-3}$ $s^{-1}$ at strain amplitudes of (a) ±0.25%, (b) ±0.50%.

The average inter striation spacing (stage II fatigue crack growth) was measured from different images and regions on the fracture surfaces, at all the strain amplitudes. The fatigue crack growth at strain rate of $10^{-2}$ $s^{-1}$ and at strain amplitudes of ±0.25% ±0.375% and ±0.50% are found to be 0.295 µm, 0.516 µm, and 0.6 µm respectively. Thus, there is increase in fatigue crack growth rate with increase in strain amplitude (Fig. 6.9). At the lowest strain amplitude of ±0.25% and at strain rate of $10^{-2}$ $s^{-1}$ fracture

surface appears to be more brittle in nature in comparison with that resulting at higher strain amplitudes.

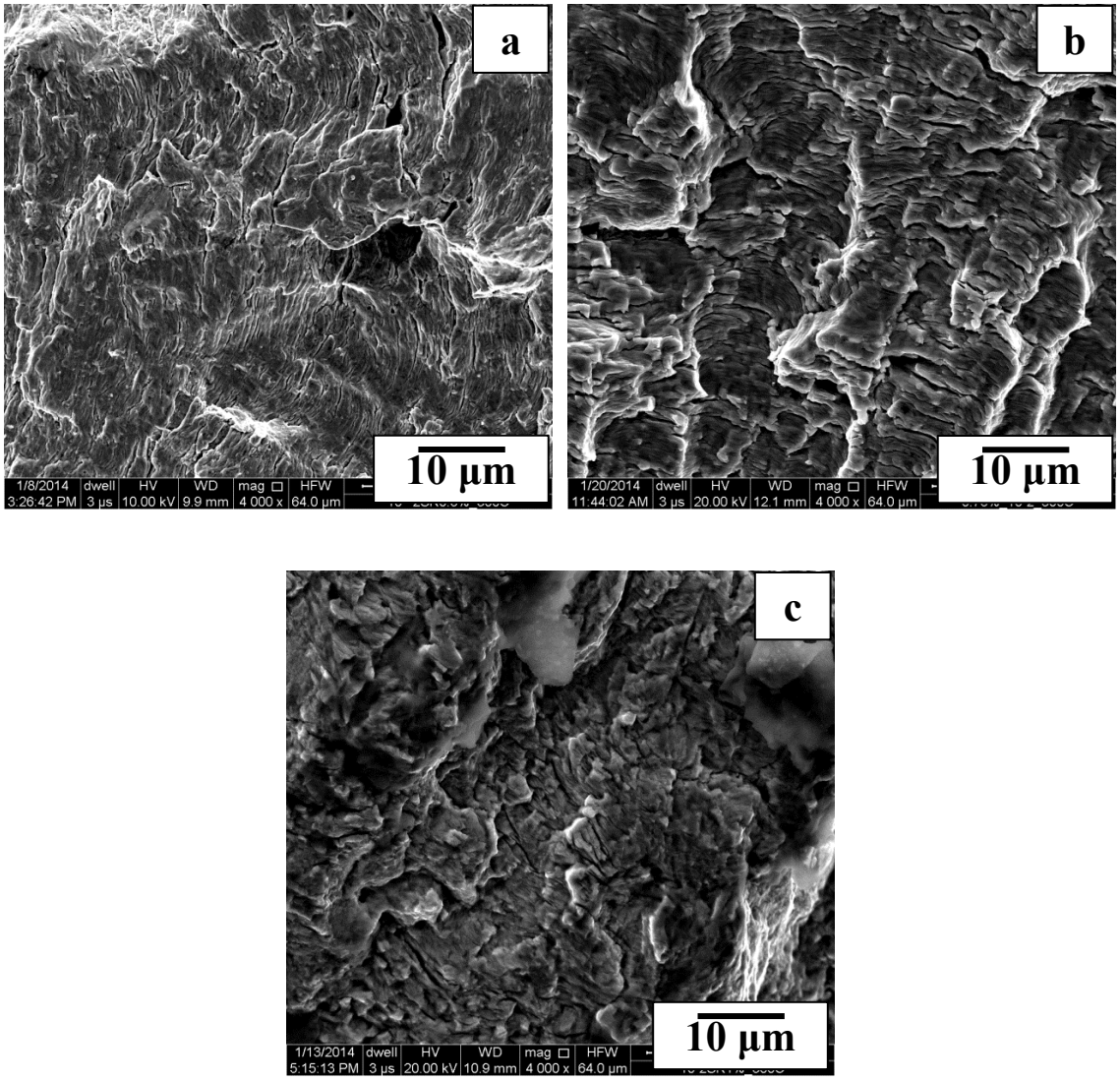


**Fig. 6.9** Magnified view of the crack propagation region at strain rate of $10^{-2}$ $s^{-1}$ at different strain amplitudes: (a) ±0.25%, (b) ±0.375%, & (c) ±0.50%.

The average inter striation spacing of stage II fatigue crack growth was determined also for the strain rate of $10^{-3}$ $s^{-1}$ and it is found to be 0.668 µm, 0.64 µm and 0.589 µm for the strain amplitudes of ±0.25%, ±0.375% and ±0.50% respectively (Fig. 6.10). It may be seen that the rate of crack growth was increased with decrease in

strain amplitude. Higher crack growth rates at lower strain rates may be seen in comparison with that at the higher strain rate of $10^{-2}$ $s^{-1}$. Thus, the lower fatigue live at the lower strain rate may be attributed to DSA.

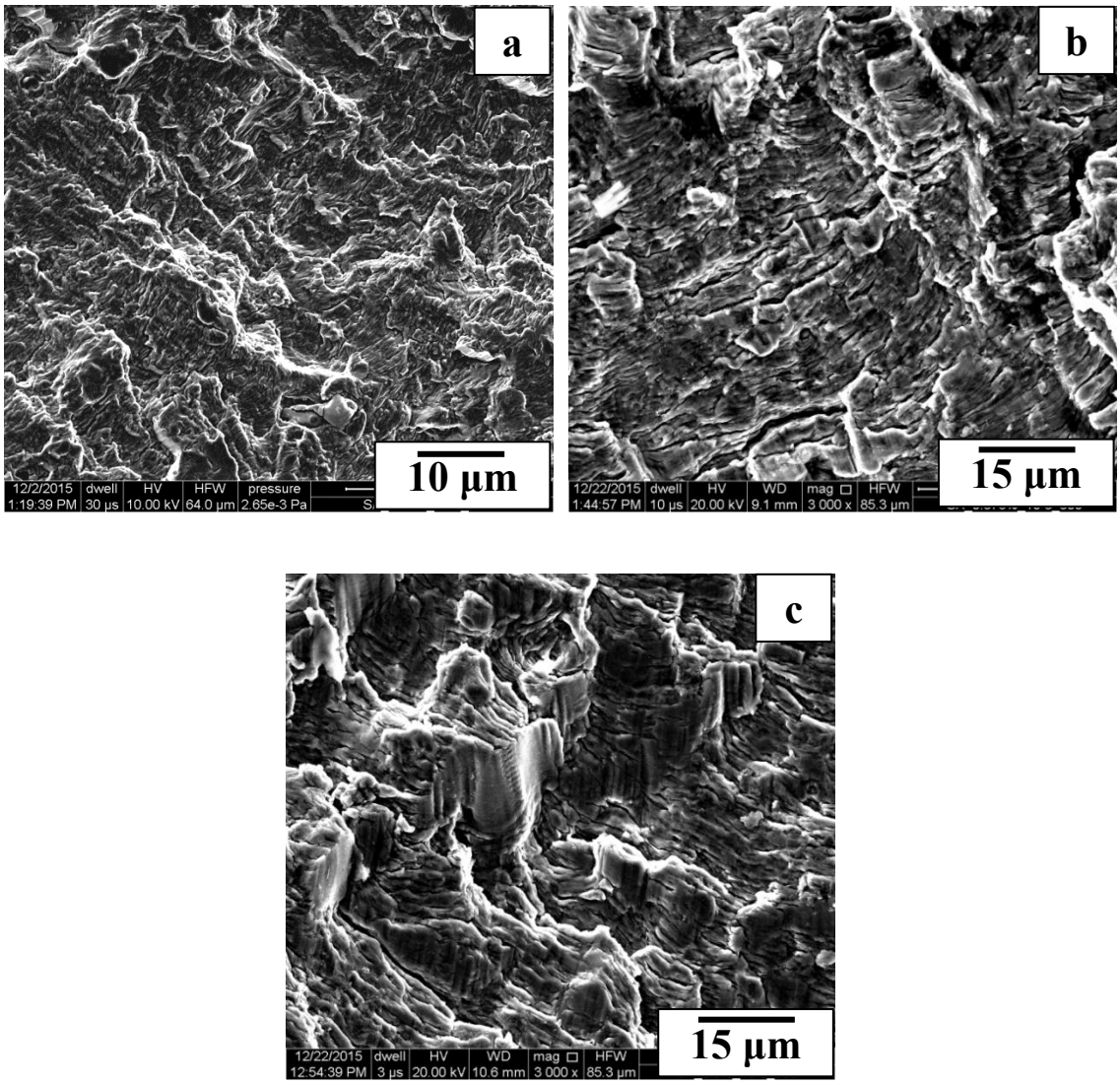


**Fig. 6.10** Magnified view of the crack propagation region at strain rate of $10^{-3}$ $s^{-1}$ at different strain amplitudes: (a) ±0.25%, (b) ±0.375%, & (c) ±0.50%.

Tire marks are observed at all the strain amplitudes except at the very low strain amplitude, and the extent of tire cracking is increased with increase in strain amplitude (Fig. 6.11). Irrespective of the strain amplitude there is occurrence of secondary cracks on the fracture surface.

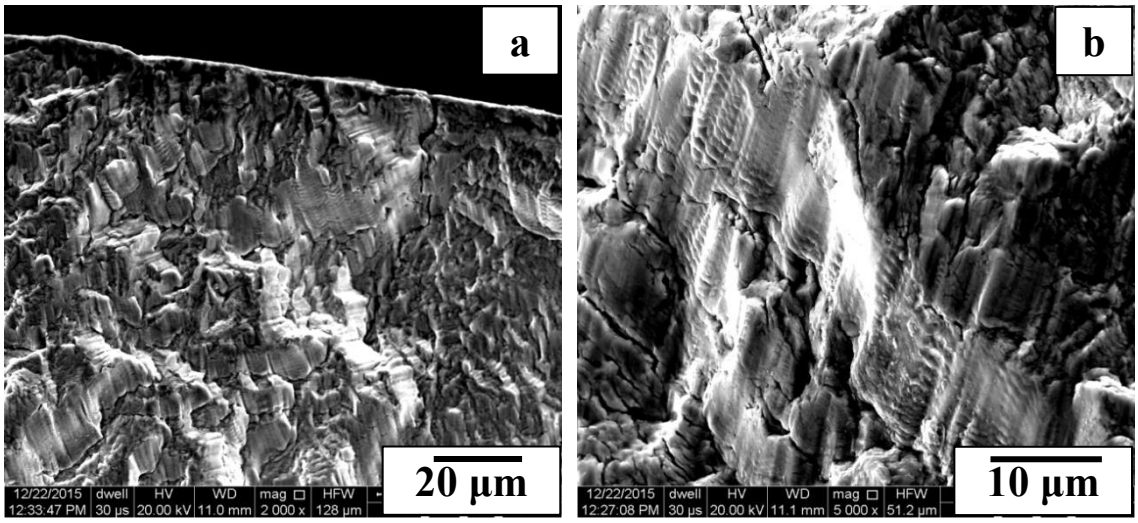


**Fig. 6.11** Tire marks at strain amplitude of ±0.50% at low strain rate of $10^{-3}$ $s^{-1}$.

## 6.7 Discussion

Usually annealed/soft metallic materials exhibit cyclic hardening while cold worked/hard materials display cyclic softening. The modified 9Cr–1Mo steel in normalized and tempered condition showed high dislocation density within the laths and at lath boundaries (Fig. 3.1c & d). This steel exhibits softening during cyclic deformation at all the strain amplitudes at both the strain rates at 300 °C (Fig. 6.1). There is formation of cell structure in this steel at 300 °C, irrespective of strain amplitude and strain rate, however, cell size is found to be dependent on strain amplitude and increases with increase in strain amplitude (Figs. 6.5 & 6.6). Thus, the observed cyclic softening in this steel may be attributed to transformation of the tempered lath structure with high density of dislocations to low energy cell structure (Figs. 6.5 & 6.6). Dynamic recovery was also seen by the annihilation of dislocations and it also promotes cyclic softening in the material (Fig. 6.12). These results are in agreement with the earlier studies [65,66,78,82].

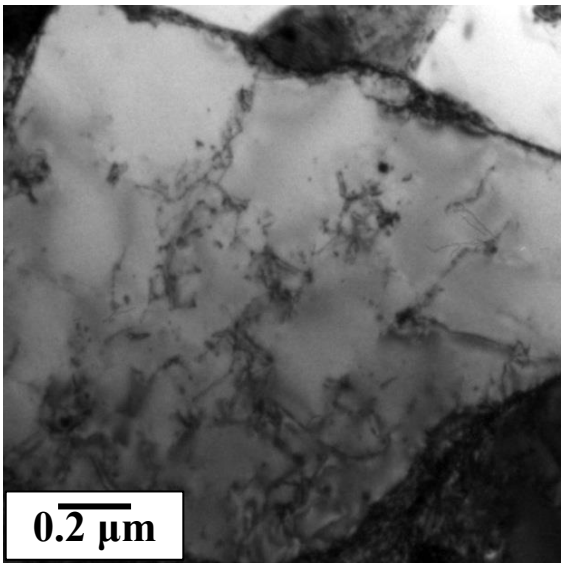


**Fig. 6.12** Bright field TEM micrographs of the specimen tested at strain amplitude of ±0.375% at strain rate of $10^{-3}$ $s^{-1}$ showing dynamic recovery.

In general, the cyclic stress amplitude decreases with decrease in strain rate. But in the present investigation an inverse effect of strain rate is observed on cyclic stress response of the modified 9Cr–1Mo steel (Fig. 6.2). The cyclic stress increased at low strain rate of $10^{-3}$ $s^{-1}$ in comparison with that at the high strain rate of $10^{-2}$ $s^{-1}$. It is important to mention that DSA in monotonic tensile loading was observed between 250–450 °C in this steel. Thus, the inverse effect of strain rate on cyclic stress response may be attributed to DSA at this temperature. Further, both fatigue life and plastic strain amplitude decreased at low strain rate of $10^{-3}$ $s^{-1}$ (Table 3.1) and also the extent of initial cyclic hardening is increased. There are several manifestations of DSA during total strain controlled LCF tests, such as serrations in stress–strain hysteresis loops, enhanced cyclic work hardening, reduced plastic strain amplitude and increase in stress response with decrease in strain rate or increase in temperature [47,151]. The occurrence of serrated flow is not a necessary requisite for characterization of DSA. It has been reported that DSA commenced earlier than it is manifested in the form of serrations in cyclic stress–strain curves in 304 SS [47]. The absence of serrations in hysteresis loops

may thus be understood (Fig. 6.4). Bowing of dislocations at low strain rate is quite obvious from the bright field TEM micrograph (Fig. 6.13).

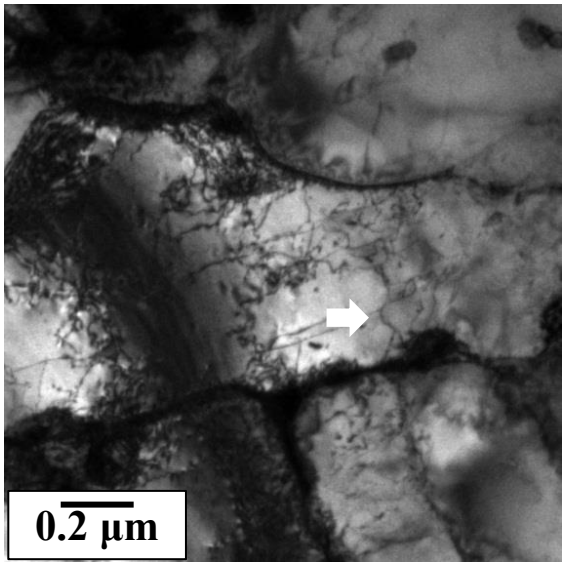


**Fig. 6.13** Bowing of dislocations may be seen from the specimen tested at strain amplitude of ±0.375% at strain rate of $10^{-3}$ $s^{-1}$.

Occurrence of DSA in the present investigation is in agreement with the earlier observation made on the modified 9Cr–1Mo steel at strain amplitude of ±0.60% at strain rate of $3 \times 10^{-3}$ $s^{-1}$ [152]. It was reported that half–life stress was increased in the temperature range from 300 to 400 °C due to DSA [152]. The decrease in fatigue life at low strain rate may be expected from increased fatigue damage per cycle resulting partially from decrease in plastic strain amplitude and consequent increase in stress amplitude [151]. The high value of stress amplitude reduced the critical crack size required for final fracture and resulted in low fatigue life [153]. The higher work hardening rates during DSA in monotonic tension may be associated with increased rates of dislocation accumulation [47,154–157]. Thus high rate of cyclic hardening at low strain rate of $10^{-3}$ $s^{-1}$ (Fig. 6.2) may be associated with increased rate of dislocation

storage due to DSA. It is also mentioned that DSA would enhance inhomogeneity of deformation during fatigue due to solute locking of the slow moving dislocations between the slip bands. Also grain boundary regions act as preferred sites for the occurrence of DSA, [157–160]. It further leads to inhomogeneity of deformation.

In the modified 9Cr–1Mo steel cell structure is observed at both strain rates and strain amplitudes at 300 °C and also at RT. Thus, it is clear that mode of deformation was cross–slip in both DSA and non–DSA region. These results are in agreement with the study of Zhou et al. [80] on effect of DSA pretreatment on LCF behavior in modified 9Cr–1Mo steel. However, in case of austenitic stainless steels, the mechanism of cyclic deformation changed from the cross–slip mode in the non–DSA region to planar slip in the DSA regime, which resulted in transformation of cell structure from a cell structure to planar one. Thus, it may be understood that DSA does not change the mode of deformation in ferritic–martensitic steel.

The process of DSA induces hardening in the material. It results in development of higher stress for a given strain amplitude at low strain rate in comparison with that at high strain rate. Therefore, a higher degree of stress concentration at the crack tip, in the regime of DSA, will enhance the crack propagation rate and lead to reduction in crack propagation life [161]. The rate of crack propagation in 316L (N) and Ferrovac E iron was significantly increased in the regime of DSA, compared with that in the non–DSA regime, because DSA–induced embrittlement restricting plasticity at the crack tip and, thus, retarded blunting of the propagating crack, to result in a higher rate of crack propagation [162,163]. The inter striation spacing or fatigue crack growth rate in stage II was found to be higher at low strain rate may be attributed to DSA (Fig. 6.9 & 6.10).

DSA reduced the crack initiation and propagation life by way of multiple crack initiation, resulting from DSA induced inhomogeneity of deformation, and rapid crack

propagation from DSA induced hardening [161]. The area of fatigue failure comprises of both crack initiation and crack propagation, it decreases and multiple crack initiation sites formed at the lower strain rate than that at the higher strain rate, at identical strain amplitude (Fig. 6.7 & 6.8). DSA localizes fatigue deformation, enhances fatigue cracking and reduces fatigue life.

Figure 6.4 shows that modified 9Cr–1Mo steel exhibits non–Masing behavior at low strain amplitude of ±0.25% and Masing behavior at higher strain amplitudes (±0.375% & ±0.50%). The dependency of strain amplitude on Masing and non–Masing behavior is found to be similar to that at RT study at different strain rates ($10^{-2}$ $s^{-1}$ to $10^{-4}$ $s^{-1}$). The transition from non–Masing to Masing behavior may be due to change in dislocation configuration from equiaxed or ill–defined cell structure at low strain amplitude to elongated and well defined cell structure at higher strain amplitudes. The non–Masing behavior in general is attributed to phase instability and transient dislocation substructure [164,165].

## 6.8 Conclusions

The following conclusions may be drawn from the present chapter:

- The modified 9Cr–1Mo steel exhibits cyclic softening at strain rates of both of $10^{-2}$ $s^{-1}$ and $10^{-3}$ $s^{-1}$ for all the strain amplitudes studied in the range ±0.25% to ±0.50%. This is attributed to formation of cell structure and occurrence of dynamic recovery.
- Inverse effect of strain rate on cyclic stress response, plastic strain amplitude and fatigue life suggests occurrence of dynamic strain ageing under cyclic deformation at 300 °C. Bowing of dislocation was also observed at the strain rate of $10^{-3}$ $s^{-1}$.

- Decrease in fatigue life at $10^{-3}$ $s^{-1}$ may be due to increase in fatigue crack growth rate manifested by increase in inter striation spacing due to DSA.
- Equiaxed cell structure at the lowest strain amplitude of ±0.25% is transformed to elongated cell structure at higher strain amplitudes (≥ ±0.375%). This could be the cause of transition of non–Masing to Masing behavior.